International Journal of Heat and Fluid Flow 30 (2009) 831–841

Contents lists available at ScienceDirect

International Journal of Heat and Fluid Flow

journal homepage: www.elsevier.com/locate/ijhff

Experimental study on bubble velocity, void fraction and pressure drop for gas–liquid two-phase flow in a circular microchannel ☆

Akimaro Kawahara *, Michio Sadatomi, Keitaro Nei, Hideki Matsuo

Dept. of Mechanical System Engineering, Kumamoto University, Kurokami 2-39-1, Kumamoto City 860-8555, Japan

ARTICLE INFO

Article history:
Received 28 October 2008
Received in revised form 27 February 2009
Accepted 28 February 2009
Available online 3 April 2009

Keywords:
Microchannel
Two-phase flow
Bubble velocity
Bubble length
Void fraction
Pressure drop

ABSTRACT

An adiabatic experiment was conducted to investigate the effects of liquid properties on the characteristics of two-phase flows in a horizontal circular microchannel. Distilled water and aqueous solutions of ethanol were used as the test liquids. The ethanol concentration was varied to change the surface tension and the viscosity. One of the four liquids together with nitrogen gas was injected through a T-junction mixer to the test microchannel. Two mixers with different inner diameters of $D_M = 250\ \mu m$ and $500\ \mu m$ were used at a fixed microchannel diameter of $D = 250\ \mu m$ to study flow contraction effects at the channel inlet. Bubble velocity data correlated with the drift flux model showed that the distribution parameter, C_0, increased with increasing of liquid viscosity and/or decreasing of surface tension, and C_0 for flows with the contraction was higher. The pressure drop data correlated with the Lockhart–Martinelli method showed that the two-phase friction multiplier, ϕ_L^2, for flows with the contraction was lower. From data analysis, new correlations of C_0 and ϕ_L^2 were developed with some dimensionless numbers. On void fraction prediction, two-fluid model code could predict well the data when an appropriate correlation of interfacial friction force was used.

1. Introduction

Vigorous studies are underway to understand the movement of a micro-scale fluid. Especially, the understanding of gas–liquid two-phase flow characteristics in a microchannel is essential for developing and designing micro-devices such as microreactor (Jähnisch et al., 2000), mobile type fuel cell (Yen et al., 2003) and micro-heat exchangers (Qu and Mudawar, 2003), etc. In the flow characteristics, Serizawa et al. (2002), Kawahara et al. (2002, 2003, 2004, 2005a,b, 2006), Chung et al. (2004), Chung and Kawaji (2004) and Kawaji et al. (2006) reported unique differences between the microchannel and the conventional sized channel.

Serizawa et al. (2002) conducted air–water two-phase flow experiments in 25 μm and 100 μm horizontal microchannels, and observed five flow patterns: dispersed bubbly, gas slug, liquid-ring, liquid lump and liquid droplet flows. The existence of the liquid-ring flow is a difference between the microchannel and the conventional sized channel.

Kawahara et al. (2002) and Chung and Kawaji (2004) studied two-phase flows of nitrogen gas and water through horizontal microchannels of 50–250 μm diameter, and reported significant differences in the flow pattern maps and void fraction data from the conventional sized channels. In addition, they reported the existence of flow patterns unique to microchannels, e.g., liquid-ring flow and serpentine-like gas core flow, and void fraction data showed a strong derivation from Armand (1946)-type correlation normally applicable to the conventional sized channel and mini-channel (Ali et al., 1993). Such a trend of void fraction data is in contrast with Serizawa et al. (2002) data for a 25 μm horizontal microchannel, which were well represented by the Armand type correlation.

Following to the above studies, Kawahara et al. (2006) and Kawaji et al. (2006) conducted adiabatic experiments to clarify the effects of gas and liquid injection methods and inlet geometry on water/nitrogen gas two-phase flow in microchannels by changing a combination of the mixer and the microchannels. Horizontal circular microchannels of 100, 176 and 251 μm I.D. were connected in turn to one of the two mixers of 250 and 500 μm I.D. Water and nitrogen gas were used as the working fluids. Two types of flow configuration were mainly observed. They were called “quasi-homogeneous flow” and “quasi-separated flow”. Interestingly, the void fraction in the quasi-homogeneous flow was higher than that in the quasi-separated one at the same gas and liquid flow rates condition.

Some papers (e.g., Chung and Kawaji, 2004) noted that with decreasing channel size, the Bond number, Reynolds number, the capillary number all decrease. Thus, compared to two-phase flows

☆ A paper submitted for publication in the HTFFM3 special issue of the International Journal of Heat and Fluid Flow (October, 2008).

* Corresponding author. Tel./fax: +81 96 342 3753.
E-mail address: akimaro@mech.kumamoto-u.ac.jp (A. Kawahara).

0142-727X/$ - see front matter © 2009 Elsevier Inc. All rights reserved.
doi:10.1016/j.ijheatfluidflow.2009.02.017

Nomenclature

a	constant in Eq. (7)
a_{INT}	interfacial area concentration
b	constant in Eq. (14)
Bo	Bond number
C	constant in Eq. (11)
C_0	distribution parameter
C	Armand constant in Eq. (9)
Ca	Capillary number
C_D	drag coefficient
D	channel diameter
D_H	hydraulic diameter
D_M	mixer diameter
E	error
F_I	interfacial friction force per unit volume
F_W	wall friction force per unit volume
g	gravitational acceleration
j	volumetric flux
L_G	bubble length
P	pressure
Re	Reynolds number
u	mean velocity
u_R	relative velocity
V_{Gj}	drift velocity
We	Weber number
X	Lockhart–Martinelli parameter
Z	axial distance

Greek symbols

α	void fraction
β	homogeneous void fraction
ϕ_L^2	two-phase friction multiplier
μ	dynamic viscosity
ρ	density
σ	surface tension

Subscripts

Cal.	calculation
Exp.	experiment
G	gas phase
L	liquid phase
m	mean
rms	root-mean-square
TP	two-phase

in conventional sized channel, the flow in microchannel seems to be more influenced by surface tension effect and viscous force rather than gravity force and inertia. In order to develop devices utilizing such a microchannel, therefore, it is essential to know the effect of surface tension and/or viscosity on two-phase flow pattern, void fraction and pressure drop etc. However, the effects have not yet been revealed because most of the two-phase flow experiments in microchannels have been performed using water alone as the working liquid.

In this connection, the purpose of this study is to know experimentally the effects of liquid physical properties on the two-phase flow characteristics, such as the bubble velocity, the bubble length, the void fraction and the pressure drop. An adiabatic experiment was conducted to obtain such characteristic data for gas–liquid two-phase flows in a 250 μm circular microchannel. In order to study effects of surface tension and viscosity, aqueous solutions of ethanol having different mass concentrations of 0, 4.8, 49 and 100 wt% were used as the working liquid, while nitrogen gas as the working gas. In addition, to know the effects of flow contraction at the channel inlet, two mixers of different inner diameters of D_M = 250 μm and 500 μm were used at a fixed microchannel diameter of D = 250 μm. In the analysis, the void fraction and pressure drop correlations reported so far are tested against the present data. Furthermore, on the void fraction, calculated value by a one-dimensional two-fluid model code is also tested. Results of the experiment and the analysis are presented in this paper.

2. Experiments

2.1. Test apparatus

Fig. 1 is the present test apparatus, being the same as that used in our previous study (Kawahara et al., 2006; Kawaji et al., 2006). As the test fluids, distilled water and aqueous solution of ethanol were used for the liquid phase, while nitrogen for the gas phase. The liquid was introduced to horizontal, circular microchannel by a pneumatic-type pump. The pump consisted of a pressure vessel containing one of the test liquids and a gas cylinder of dry nitrogen for pushing the liquid surface in the vessel. This pump gave a stable and pulsation-free liquid flow. All tubing and fittings were made of stainless steel or brass to avoid any volumetric expansion in the flow loop and fluids leakage by a high pressure. A gas and liquid mixture made at a mixer flowed through the circular microchannel test section and discharged to the atmosphere.

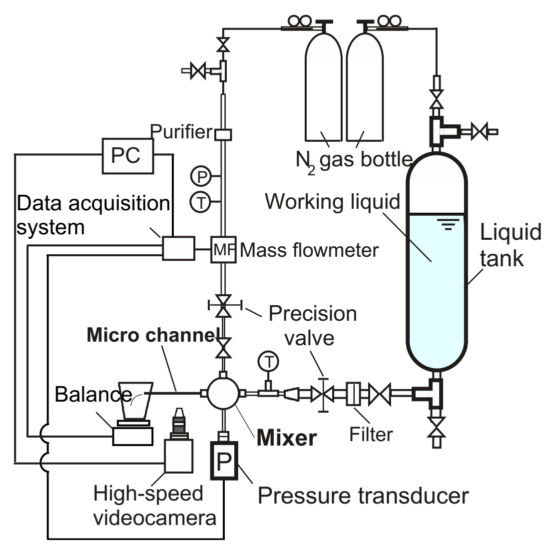

Fig. 1. Test apparatus.

The liquid flow rate was determined by weighing the liquid discharged in a small container over a sufficient period of time with an electronic balance (200 ± 0.001 g, SHIMADZU Co.). The gas flow rate was read from a calibrated mass flow meter (5 SCCM, Type HM5111B, Tokyo Keiso Co., Ltd.).

The transparent test section made of a 250 μm I.D. fused silica (Polymicro Technologies Inc.) enabled us to observe flow with a high speed video camera (Hi-Dcam PCI 8000S, NAC Image Technology). Background illumination was provided by a high-intensity

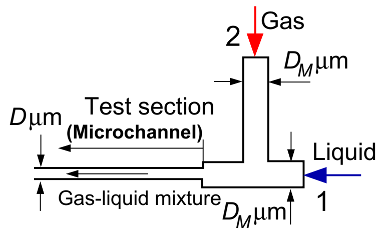

Fig. 2. Gas–liquid mixer and the microchannel.

luminescent lamp (LA-180Me, Hayashi Tokei Kogyo Co.) and gooseneck light guide placed behind the test section. To record enlarged images of the flow inside the test section, a macro zoom lens (Z16APO, Leica Microsystems) was coupled to the video camera as shown in Fig. 1. The total length of the microchannel was $L = 99$ mm, and a high L/D ratio ($L/D = 396$) allowed us to diminish the entrance and exit effects. The window for the flow observation was located at the mid point of the test section.

Fig. 2 shows a gas–liquid mixer made from a T-junction (Valco Instrument Co., Inc.) with an inner diameter of $D_M = 250$ or 500 µm. Since the T-junction was directly connected to the 250 µm I.D. test section, when 500 µm I.D. mixer was used, flow contraction occurred at the inlet of the test section. Liquid was injected into the main channel (line 1), while the gas into the branch (line 2).

2.2. Bubble velocity, bubble length and void fraction measurement

The high speed video camera was used to determine velocity and length of the bubbles in the test section. The images of flow with a resolution of 160 × 78 pixels were recorded at 8000 frames per second and at a shutter speed of 1/160,000 s. The recorded images were transmitted to a computer for image processing by a commercial software.

The bubble velocity, u_G, can be determined as

$$u_G = \Delta Z f. \tag{1}$$

Here, f is the frame rate of the video camera and ΔZ the moving distance of the bubble nose during $1/f$.

The bubble length, L_G, was determined by measuring the distance from the nose of the bubble to the tail if the bubble length was shorter than an image width (ca. 2.6 mm). If the bubble length was longer than the image width, L_G was determined by Agostini et al.'s method (2008):

$$L_G = u_G(F_{t,i} - F_{n,o})/f. \tag{2}$$

Here, $F_{t,i}$ is the frame number when the bubble tail appears on the video image, $F_{n,o}$ the frame number when the bubble nose disappears on the video image.

The void fraction, α, was determined by substituting u_G data into:

$$\alpha = j_G/u_G. \tag{3}$$

Here, j_G is the volumetric flux of the gas phase at the mid point of the test section.

2.3. Determination of frictional pressure drop

The pressure drop measured in the present experiment, $\Delta P_{\text{measured}}$, is the sum of three components:

$$\Delta P_{\text{measured}} = \Delta P_{\text{friction}} + \Delta P_{\text{contraction}} + \Delta P_{\text{acceleration}}. \tag{4}$$

Here, $\Delta P_{\text{friction}}$ is the component of wall friction, $\Delta P_{\text{contraction}}$ that of contraction at the microchannel inlet, and $\Delta P_{\text{acceleration}}$ that of acceleration due to the expansion of the gas phase. In order to obtain the frictional component, the second and the third components on the right hand side of Eq. (4) must be subtracted from the pressure drop measured with a calibrated pressure transducer (FP101 Series, Yokogawa Co.). For that purpose, $\Delta P_{\text{contraction}}$ and $\Delta P_{\text{acceleration}}$ were estimated from a method described in Kawahara et al. (2002). The results showed that the contributions of the contraction and the acceleration components to the total pressure drop were, respectively 0.01% to 1.26% and 0.001% to 0.2%, depending on the flow conditions.

2.4. Experimental conditions

Distilled water, aqueous solutions of ethanol with two different mass concentrations (49 wt% and 4.8 wt%) and pure ethanol were used as the working liquid. The density, dynamic viscosity and surface tension of each liquid are listed in Table 1. The deviation from the mean value depends on the change in liquid temperature in the experiments. A peculiar dependency of viscosity on the ethanol concentration is seen; it takes a maximum value at 49 wt%, and takes almost the same value at 100 wt% and 4.8 wt% though they are about three times different in surface tension.

The ranges of liquid and gas volumetric fluxes, j_L and j_G, are shown in Table 2. It should be noted that the volumetric flux of the gas phase was calculated using a gas density at the mid point of the test section which was evaluated by the system pressure and liquid temperature there.

The ranges of dimensionless numbers related to the present experiments are shown in Table 3. The significance of inertia force to viscous force is known from the liquid and the gas Reynolds numbers, $Re_L(=\rho_L j_L D/\mu_L)$ and $Re_G(=\rho_G j_G D/\mu_G)$, while that of inertia force to surface tension force is indicated from the Weber numbers, $We_L(=\rho_L j_L^2 D/\sigma)$ and $We_G(=\rho_G j_G^2 D/\sigma)$. That of gravity force to surface tension force, the Bond number, $Bo(=(\rho_L - \rho_G)gD^2/\sigma)$, was much smaller than unity in the present experiment. That of viscous force to surface tension force, the capillary number, $Ca(=\mu_L j_L/\sigma)$, was from 0.0024 to 0.851.

3. Experimental results and discussions

3.1. Flow pattern

Figs. 3 and 4 show typical flow without the flow contraction at the microchannel inlet, respectively for different working liquids.

Table 1
Properties of working liquids.

Working liquids	Density ρ_L (kg/m^3)	Viscosity μ_L (mPa s)	Surface tension σ (N/m)
Distilled water	996.5 ± 1.7	0.92 ± 0.1	0.072 ± 0.001
Ethanol 4.8 wt%	989.4 ± 1.6	1.19 ± 0.2	0.060 ± 0.001
Ethanol 49 wt%	910.9 ± 5.3	2.43 ± 0.5	0.028 ± 0.001
Ethanol 100 wt%	785.7 ± 7.5	1.16 ± 0.2	0.022 ± 0.001

Table 2
Ranges of volumetric fluxes for liquid and gas.

Working liquids	j_L (m/s)	j_G (m/s)
Distilled water	0.22–1.43	0.04–1.24
Ethanol 4.8 wt%	0.11–1.08	0.07–0.96
Ethanol 49 wt%	0.21–0.91	0.04–1.77
Ethanol 100 wt%	0.22–1.52	0.02–1.33

Table 3
Ranges of dimensionless numbers.

Working liquids	Re_L	Re_G	We_L	We_G	Bo	Ca
Distilled water	52–386	0.6–24	0.16–7.12	0.00001–0.0070	0.008	0.0026–0.018
Ethanol 4.8 wt%	20–231	1.4–22	0.05–4.18	0.00003–0.0064	0.010	0.0024–0.021
Ethanol 49 wt%	17–139	0.8–37	0.35–12.3	0.00002–0.043	0.020	0.019–0.851
Ethanol 100 wt%	33–287	0.5–26	0.41–20.9	0.00001–0.029	0.022	0.012–0.56

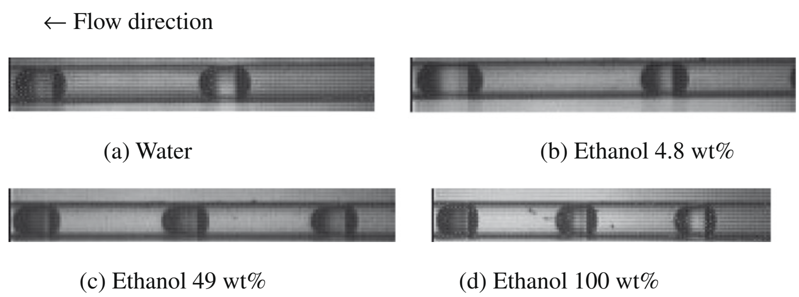

Fig. 3. Quasi-homogeneous flow observed for flows without flow contraction at j_L = 0.4 m/s and j_G = 0.1 m/s.

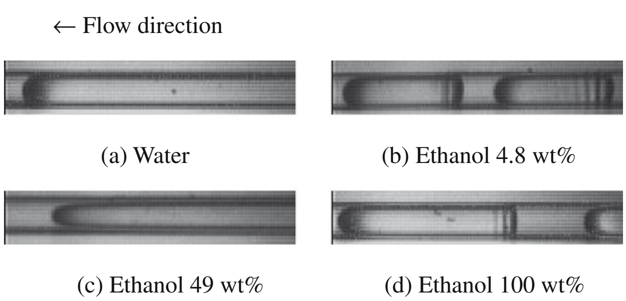

Fig. 4. Quasi-separated flow observed for flows without flow contraction at j_L = 0.4 m/s and j_G = 1.0 m/s.

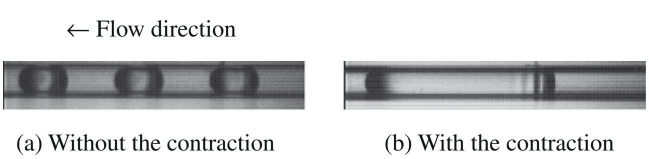

Fig. 5. Effect of the flow contraction at j_L = 0.8 m/s and j_G = 0.4 m/s for water case.

Two types of flow pattern were observed. The first one, which is called as a quasi-homogeneous flow (Kawahara et al., 2006; Kawaji et al., 2006), is featured by the presence of gas plugs shorter than the width of viewing window (ca. 2.6 mm) as shown in Fig. 3. The second one, called as a quasi-separated flow (Kawahara et al., 2006; Kawaji et al., 2006), is characterized by a longer gas bubble surrounded by a smooth or a wavy liquid film, as shown in Fig. 4. The quasi-homogeneous flow tends to occur at relatively high liquid flux, while the quasi-separated flow at relatively low liquid and/or high gas fluxes.

Fig. 5 shows the effects of the flow contraction on the flow pattern. You can see longer bubbles for flows with the contraction even at the same gas and liquid flow rates condition.

3.2. Bubble velocity

Fig. 6a–d show the bubble velocity data, u_G, plotted against the total volumetric flux, $j(=j_G+j_L)$, for flows without and with the flow contraction. The open symbol represents data for the flows without the contraction, while solid symbol for the flows with the contraction. The solid and broken lines represent regression lines of the data for the respective cases based on the well-known drift flux model (Zuber and Findlay, 1968):

$$u_G = C_0 j + V_{Gj}. \tag{5}$$

Here, C_0 is the distribution parameter and V_{Gj} the drift velocity. In the regression, V_{Gj} was taken as zero because flows in the present study were horizontal. Table 4 shows the C_0 data. From Fig. 6 and Table 4, it is found that u_G and C_0 increased with increasing of the liquid viscosity and/or decreasing of the surface tension. The reason of this is probably that liquid film thickness around the gas bubble decreases with the increasing of the liquid viscosity, and the bubble nose shape become sharpen with increasing of the viscosity and/or the deceasing of the surface tension, as seen in Fig. 4. As for the contraction effects, C_0 were higher for the flows with the contraction. The reason is presumably that the contraction elongates the bubble in the central region of the channel, and the bubble flows faster.

For air–water two-phase flow in vertical circular pipes of 1–5 mm I.D., Mishima and Hibiki (1996) obtained the following C_0 correlation:

$$C_0 = 1.2 + 0.510\exp(-0.691D). \tag{6}$$

The substitution of D = 0.25 mm into Eq. (6) yields C_0 = 1.62, being much higher than C_0 = 1.10–1.22 for water case in the present data. Thus, there is a room of improvement in Eq. (6) for flows of different working fluids in smaller channels than 1 mm I.D.

In order to develop the C_0 correlation applicable to the different liquids–gas flows, the present C_0 data were tried to correlate with various dimensionless numbers, and finally the following equation was obtained:

$$C_0 = aBo^{0.19}Re_L^{-0.01}We_G^{0.01}. \tag{7}$$

In Eq. (7), the constant a depends on flows without and with the contraction, i.e., a = 3.0 for the flow without the contraction, a = 3.3 for the flow with the contraction. Fig. 7a and b shows comparison of u_G between experiment and calculation by Eqs. (5) and (7). The calculations agreed well with the data for all the test liquids within r.m.s errors of 11.4%, irrespective of the flows without and with the contraction.

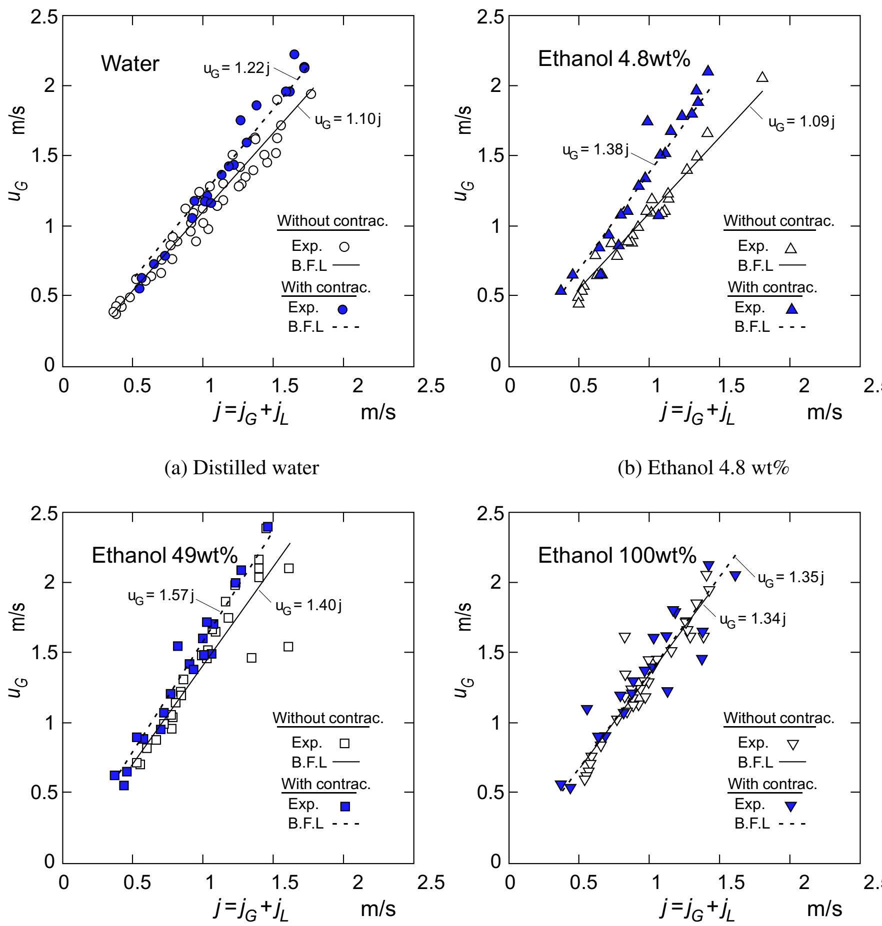

(a) Distilled water (b) Ethanol 4.8 wt%

(c) Ethanol 49 wt% (d) Ethanol 100 wt%

Fig. 6. Bubble velocity for four-kinds of test liquids–nitrogen gas two-phase flows without and with contraction.

Table 4
Distribution parameter data for the present channel.

	Water	Ethanol 4.8 wt%	Ethanol 49 wt%	Ethanol 100 wt%
Without contraction	1.10	1.09	1.40	1.34
With contraction	1.22	1.38	1.57	1.35

3.3. Bubble length

Fig. 8 shows the bubble length, L_G, data plotted against the homogeneous void fraction, $\beta(=j_G/(j_G+j_L))$, for the respective working liquid flows without and with the flow contraction. Significant contraction effects on L_G can be seen, that is, L_G is longer for flows with the contraction even in the same homogeneous void fraction, β, in $\beta < 0.6$. For flows with the contraction, L_G shows big scatters, depending mainly on liquid viscosity difference. However, for flows without the contraction, the scatter becomes small, and L_G is less than the channel inner diameter in $\beta < 0.2$, and increases with β.

The elongation of bubbles for flows with the contraction can be explained qualitatively as follows. Larger gas bubbles would be produced in the T-junction of $D_M = 500$ μm by a step upstream of the microchannel test section. When these bubbles are periodically released over the step and flow into the microchannel with a smaller diameter ($D = 250$ μm), the bubble length must be increased by four times. For example, if the length of the gas bubble in the T-junction were 500 μm, it would become a 2 mm in the microchanel.

3.4. Void fraction

Fig. 9 presents the void fraction, α, data plotted against the homogeneous void fraction, β, for different working liquid flows without the flow contraction. For comparison, a dot-dash curve calculated by Kawahara et al.'s correlation (2002), Eq. (8), for nitrogen gas/water flow in a 100 μm circular channel, is drawn on the figure.

$$\alpha = \frac{0.03\beta^{0.5}}{1-0.97\beta^{0.5}}. \tag{8}$$

In addition, two lines corresponding to a homogeneous flow line ($\alpha = \beta$) and Armand's correlation (1946):

$$\alpha = \frac{1}{C_A}\beta, \quad C_A = 1.2, \tag{9}$$

are, respectively shown by solid and dashed lines. Ali et al. (1993) recommended the use of an Armand type correlation ($\alpha = 0.8\beta$) for narrow rectangular channels with $D_H \sim 1$ mm.

The void fraction data for distilled water and 4.8 wt% ethanol solution distributed between the lines for homogeneous flow model and Armand correlation. The data for 49 wt% ethanol solution and pure ethanol is lower than data for the above two test liquids.

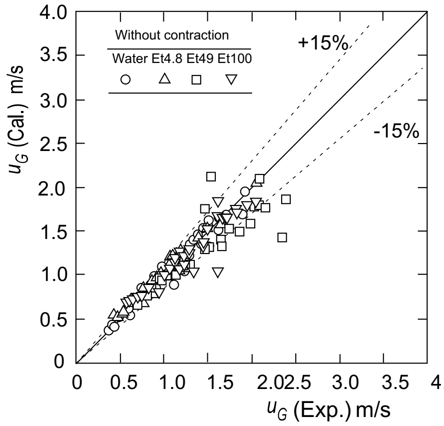

(a) Without contraction

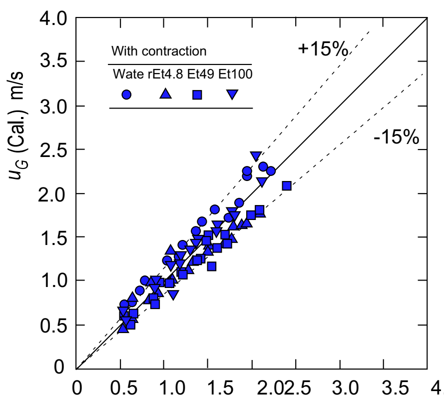

(b) with contraction

Fig. 7. Comparison of bubble velocity between experiment and calculation by Eqs. (5) and (8).

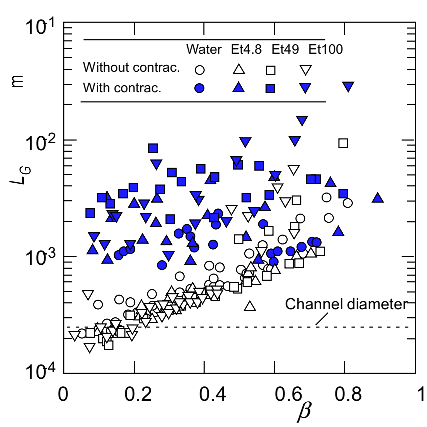

Fig. 8. Bubble length against homogeneous void fraction.

In addition, the data for 49 wt% ethanol solution, having the highest viscosity among the test liquids, tend to approach the curve by Eq. (8).

In order to know the effects of the flow contraction on the void fraction, Fig. 10 compares void fraction data for 49 wt% ethanol solution flows without and with the contraction. The data for flows with the contraction were lower than that without the contraction at the same homogeneous void fraction, β, and apt to approach the curve by Eq. (8). The reason is presumably that the contraction elongates the bubble in the central region of the channel as shown in Figs. 5 and 8, and makes the bubble velocity faster.

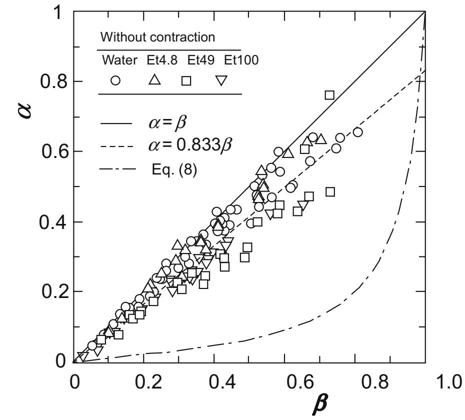

Fig. 9. Void fraction for four-kinds of test liquids–nitrogen gas two-phase flow without contraction – effects of liquid properties on void fraction.

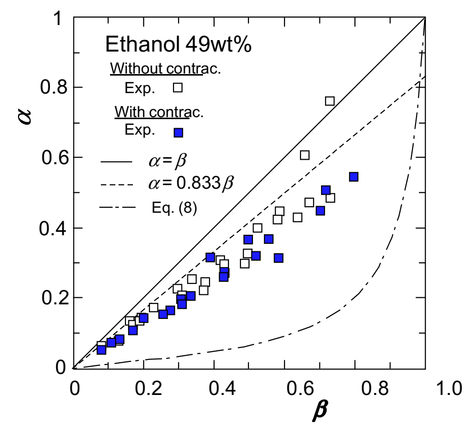

Fig. 10. Void fraction for ethanol 49 wt% aqueous solution–nitrogen gas two-phase flow – effects of the contraction on void fraction.

3.5. Two-phase frictional pressure drop

The frictional pressure drop data are commonly correlated with the following two-phase friction multiplier, φ_L^2 (Lockhart and Martinelli, 1949):

$$\left(\frac{dP_f}{dZ}\right)_{TP} = \phi_L^2 \left(\frac{dP_f}{dZ}\right)_L, \tag{10}$$

where $(dP_f/dZ)_L$ is the frictional pressure drop when the liquid in two-phases flows alone in the same channel. A widely used correlation for the friction multiplier is that proposed by Chisholm and Laird (1958),

$$\phi_L^2 = 1 + \frac{C}{X} + \frac{1}{X^2}, \tag{11}$$

where X is the Lockhart–Martinelli parameter given by

$$X^2 = \frac{(dP_f/dZ)_L}{(dP_f/dZ)_G}. \tag{12}$$

In Eq. (12), $(dP_f/dZ)_G$ is the frictional pressure drop when the gas flows alone in the same channel.

The coefficient, C, in Eq. (11) is the constant ranging from 5 to 20 in conventional sized channels, depending on whether flows of the liquid and the gas are laminar or turbulent. According to Chisholm and Laird's criteria, the value of C for the present flow conditions must be five, because both the liquid and the gas are in laminar flow, i.e., $Re_L(=\rho_L j_L D/\mu_L) < 3860$ and $Re_G(=\rho_G j_G D/\mu_G) < 2370$.

Mishima and Hibiki (1996) proposed a correlation of the C-value for their data on air–water flow in circular and rectangular channels of $D_H = 1$–4 mm as well as the data reported by other researchers:

$$C = 21(1 - e^{-0.319D_H}), \tag{13}$$

where D_H is the hydraulic diameter of the channel.

Fig. 11 shows a comparison of the two-phase friction multiplier data with the predictions by Eq. (11) with $C = 5$ and $C = 1.61$ given by Eq. (13). Also shown in the same figure is the calculated curve by Kawahara et al. (2002) with $C = 0.24$ for nitrogen gas/deionised water two-phase flow in a 100 μm circular channel. The data are well correlated with the Lockhart–Martinelli parameter, and an appropriate C-value seems to depend on the flow contraction. For flows with the contraction, the data agree reasonably with the calculation with $C = 1.61$, irrespective of the working liquids. For the flows without the contraction, on the other side, the data distribute around the calculation with $C = 5$. The reason why the friction multiplier is higher for flows without the contraction is as follows: For the flows without the contraction, the void fraction is higher as mentioned before, thus, mean liquid velocity, $u_L = j_L/(1 - \alpha)$, is faster, and resulting the wall friction higher.

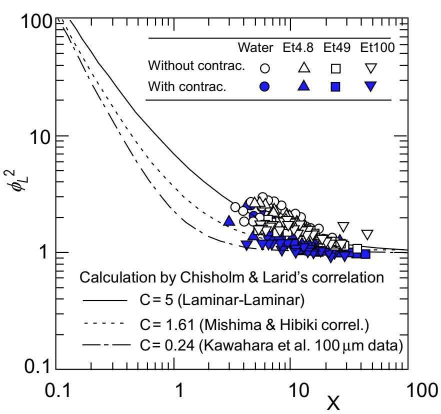

Fig. 11. Two-phase friction multiplier versus Lockhart–Martinelli parameter.

The liquid properties seem to affect the C-value. So, the C data were obtained from the present frictional pressure drop data. The resulting C data were tried to correlate with three dimensionless numbers, and finally Eq. (14) was obtained:

$$C = bBo^{0.04}Re_L^{0.25}We_G^{-0.12}. \tag{14}$$

In Eq. (14), the constant b depends on the flows without and with the contraction, i.e., $b = 1.38$ for the flow without the contraction, $b = 0.55$ for the flow with the contraction. Fig. 12a and b presents a comparison of two-phase frictional multiplier between the experiment and the calculation by Eqs. (11) and (14). The calculation agreed well with the data within 20% r.m.s. errors, irrespective of the test liquids.

4. Analysis of pressure drop and void fraction

4.1. Two-phase frictional pressure drop prediction

In this section, eleven correlations developed for both macro and mini/micro-channels are confirmed to validate their suitability to the present two-phase frictional pressure drop data. The correlations tested are: homogeneous flow model with six different viscosity models (McAdams, 1954; Owens, 1961; Cicchitti et al., 1960; Dukler et al., 1964; Beattie and Whalley, 1982; Lin et al., 1991), Lockhart and Martinelli (L–M) model with four different C models (Chisholm and Laird, 1958; Mishima and Hibiki, 1996; Lee and Lee, 2001; Qu and Mudawar, 2003), and separated flow model (Ali et al., 1993). The L–M model with a newly developed C correlation, Eq. (14), was also tested. Table 5 lists the test results. The mean error, E_m, and the RMS error, E_{rms}, are defined as

$$E_m = \left[\frac{1}{N}\sum_{i=1}^{N}\frac{(dP_f/dZ)_{TP\cdot Cal,i} - (dP_f/dZ)_{TP\cdot Exp,i}}{(dP_f/dZ)_{TP\cdot Exp,i}}\right] \times 100, \tag{15}$$

$$E_{rms} = \sqrt{\frac{1}{N-1}\sum_{i=1}^{N}\left(\frac{(dP_f/dZ)_{TP\cdot Cal,i} - (dP_f/dZ)_{TP\cdot Exp,i}}{(dP_f/dZ)_{TP\cdot Exp,i}}\right)^2} \times 100. \tag{16}$$

For flows without the contraction, L–M model with Chisholm and Laird's C model (1958) and the developed C correlation, Eq. (14), and separated flow model (Ali et al., 1993) give the best results, irrespective of working liquids. For flows with the contraction, L–M model with Mishima and Hibiki's C model (1996) and Lee and Lee's C model (2001), and the developed C correlation, Eq. (14), and homogeneous flow model with Dukler et al.'s viscos-

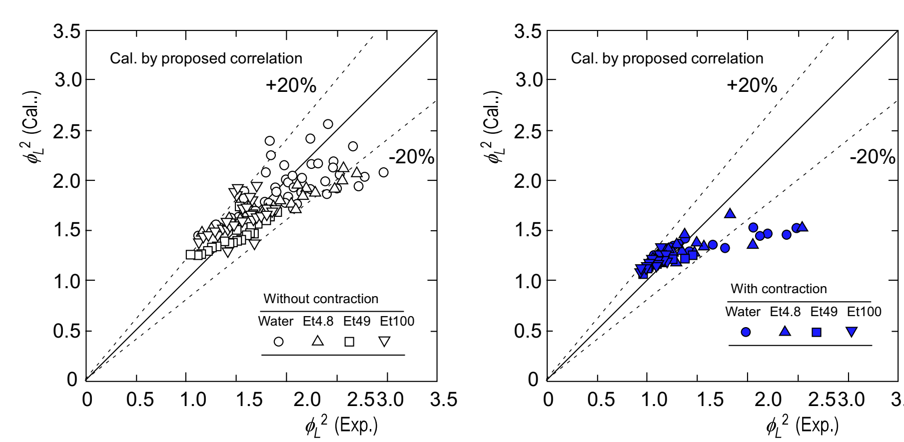

(a) Without contraction (b) With contraction

Fig. 12. Comparison of two-phase friction multiplier between experiments and calculation by Eqs. (11) and (14).

Table 5
Mean and RMS errors of various correlations for predicting two-phase frictional pressure gradient.

	Distilled water		Ethanol 4.8 wt%		Ethanol 49 wt%		Ethanol 100 wt%	
	E_m (%)	E_{rms} (%)	E_m (%)	E_{rms} (%)	E_m (%)	E_{rms} (%)	E_m (%)	E_{rms} (%)
(a) Without contraction								
Homogeneous flow type								
Owens	−7.9	36.1	−8.9	15.0	31.7	57.6	1.7	29.8
McAdams	−13.9	30.6	−14.4	17.0	8.5	23.5	−5.0	23.1
Cicchitti	−8.1	36.0	−9.0	15.0	31.4	57.1	1.6	29.7
Dukler et al.	−47.9	49.7	−43.7	46.7	−30.0	32.4	−34.9	36.5
Beattie and Whalley	−0.8	18.9	3.2	6.6	36.8	43.1	16.0	28.6
Lin et al.	−8.5	35.2	−9.4	14.9	28.7	51.9	1.1	28.9
Lockhart–Martinelli type								
Chisholm and Laird	−18.0	22.9	−16.8	19.8	−1.8	9.4	−4.9	14.1
Mishima and Hibiki	−38.3	40.2	−35.0	37.9	−20.9	23.1	−25.2	27.0
Lee and Lee	−47.8	49.5	−43.6	46.6	−30.0	32.3	−34.9	36.4
Qu and Mudawar	−26.4	29.3	−23.9	28.5	−9.3	16.1	−11.4	19.6
Eq. (14) with $b = 1.38$	−15.9	20.7	−17.0	21.6	−12.6	15.0	9.2	13.7
Separated flow model	−17.6	25.0	−13.1	15.7	2.7	30.8	−14.3	18.6
(b) With contraction								
Homogeneous flow type								
Owens	28.2	40.5	54.9	114.9	77.8	99.9	75.5	110.9
McAdams	18.0	28.0	31.5	59.1	41.0	46.6	53.1	71.2
Cicchitti	28.0	40.3	54.4	113.6	77.4	99.3	75.1	110.1
Dukler et al.	−26.7	33.9	−22.8	27.7	−2.2	10.4	−3.6	8.3
Beattie and Whalley	39.2	49.0	46.1	55.2	87.4	95.1	83.4	93.4
Lin et al.	27.2	39.2	50.6	101.6	72.7	90.9	72.6	104.5
Lockhart–Martinelli type								
Chisholm and Laird	9.4	21.6	15.8	23.9	26.0	27.2	41.2	45.4
Mishima and Hibiki	−17.2	25.8	−10.4	17.0	5.1	8.4	10.8	12.5
Lee and Lee	−29.6	36.0	−22.7	27.6	−4.8	11.0	−3.6	8.3
Qu and Mudawar	3.2	25.8	2.4	17.8	13.3	18.4	22.1	24.4
Eq. (14) with $b = 0.55$	−7.6	22.8	−0.02	15.4	8.2	11.8	17.4	18.8
Separated flow model	11.1	25.2	32.6	97.1	32.8	36.5	44.5	70.4

ity model (1964) give the best predictions, irrespective of working liquids. Besides L–M model with Eq. (14), L–M model with Qu and Mudawar's *C* model (2003) predicts reasonably well both flow data without and with the contraction, irrespective of working liquids. Figs. 13 and 14 show a graphical presentation of the prediction results by L–M method with Eq. (14) and Qu and Mudawar's *C* model (2003), respectively. The RMS error is within 30% for both flows with and without the contraction, irrespective of the test liquids, and Eq. (14) has better prediction as a result of accounting the liquid properties. The reason of the better prediction by Qu and Mudawar's *C* model is probably that the model is modified version of Mishima and Hibiki's one to incorporate the effects of mass flux based on the data in microchannel heat sink containing 21 parallel 271 × 713 μm microchannels.

4.2. Void fraction prediction

Ten traditional correlations developed for both macro- and mini/micro-channels are examined to validate their suitability for use with the present void fraction data. The correlations tested are: Armand type correlations (Armand, 1946; Chisholm, 1973; Spedding and Chen, 1986), correlations of homogeneous flow etc.

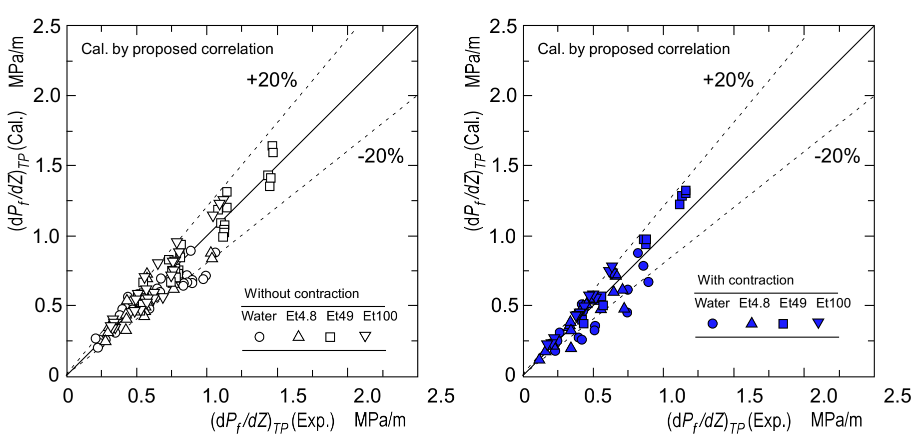

(a) Without contraction (b) With contraction

Fig. 13. Comparison of two-phase frictional pressure gradient between experiments and calculations by L–M model with a newly developed *C* correlation, Eq. (14).

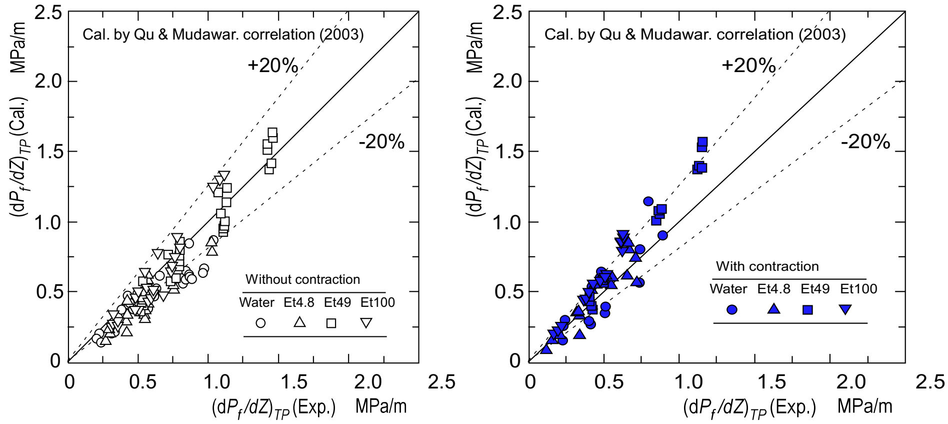

(a) Without the contraction (b) With the contraction

Fig. 14. Comparison of two-phase frictional pressure gradient between experiments and calculation by L–M model with Qu and Mudawar's *C* model (2003).

Table 6
Mean and RMS errors of various correlations for predicting void fraction.

	Distilled water		Ethanol 4.8 wt%		Ethanol 49 wt%		Ethanol 100 wt%	
	E_M	E_{RMS}	E_M	E_{RMS}	E_M	E_{RMS}	E_M	E_{RMS}
(a) Without contraction								
Armand type correlation								
Armand correlation	−0.031	0.044	−0.041	0.050	0.053	0.087	0.033	0.053
Chisholm correlation	−0.028	0.042	−0.036	0.051	0.055	0.086	0.041	0.054
Speeding and Chen	−0.031	0.044	−0.041	0.050	0.054	0.087	0.034	0.053
Butterworth type correlation								
Homogeneous flow model	0.030	0.055	0.022	0.035	0.122	0.151	0.088	0.110
Zivi model	−0.277	0.298	0.279	0.306	−0.191	0.220	−0.174	0.191
Turner and Wallis model	−0.284	0.310	−0.285	0.317	−0.208	0.242	−0.177	0.197
Lockhart and Martinelli correlation	−0.113	0.131	−0.119	0.142	−0.031	0.083	−0.019	0.042
Thom correlation	−0.203	0.217	−0.215	0.233	−0.134	0.156	−0.121	0.133
Baroczy correlation	−0.154	0.169	−0.163	0.183	−0.086	0.116	−0.070	0.083
Kawahara et al. correlation	0.050	0.057	0.008	0.035	0.004	0.063	0.090	0.098
(b) With contraction								
Armand type correlation								
Armand	−0.021	0.136	0.018	0.060	0.070	0.084	0.032	0.064
Chisholm	−0.021	0.136	0.022	0.066	0.073	0.083	0.036	0.069
Speeding and Chen	−0.021	0.136	0.019	0.060	0.070	0.084	0.032	0.064
Butterworth type correlation								
Homogeneous flow model	0.053	0.148	0.085	0.104	0.135	0.157	0.096	0.117
Zivi model	−0.290	0.334	−0.212	0.249	−0.164	0.183	−0.195	0.228
Turner and Wallis model	−0.303	0.349	−0.226	0.273	−0.180	0.207	−0.206	0.248
Lockhart and Martinelli correlation	−0.118	0.187	−0.062	0.112	−0.014	0.043	−0.037	0.087
Thom correlation	−0.209	0.255	−0.144	0.167	−0.116	0.128	−0.136	0.158
Baroczy correlation	−0.160	0.217	−0.102	0.136	−0.068	0.082	−0.088	0.120
Kawahara et al.	0.036	0.138	0.044	0.079	−0.021	0.037	0.042	0.070

seen in Butterworth's paper (1975) and Kawahara et al.'s correlation (2005b). Table 6 lists the mean error, E_M, and the RMS error, E_{RMS}, in each correlation, defined as

$$E_M = \frac{1}{N}\sum_{i=1}^{N}(\alpha_{Cal,i} - \alpha_{Exp,i}), \tag{17}$$

$$E_{RMS} = \sqrt{\frac{1}{N-1}\sum_{i=1}^{N}(\alpha_{Cal,i} - \alpha_{Exp,i})^2}. \tag{18}$$

Chisholm (1973), Armand (1946), Spedding and Chen (1986) and Kawahara et al. (2005b) correlations give better results. In more detail, Chisholm (1973), Armand (1946) and Spedding and Chen (1986) correlations tend to over-predict the data for flows with the contraction, while Kawahara et al.'s one over-predict the data for flows without the contraction. Fig. 15 shows a graphical representation of the prediction results by Kawahara et al.'s correlation (2005b). The reason of the better prediction by Kawahara et al.'s correlation is probably that the correlation was developed by using data for two-phase flows in 50–250 μm microchannels.

Two-fluid model (Ishii, 1975; Ishii and Mishima, 1984) is an up-to-date prediction method, and is used in various engineering fields. So, we tried to test the two-fluid model against the present void fraction data. In the calculation of a steady state, adiabatic flow by the two-fluid model, the following gas and liquid momentum equations were simultaneously solved:

$$\frac{d}{dZ}(\rho_G \alpha u_G^2) + F_{WG} + F_I + \alpha\frac{dP_G}{dZ} = 0, \tag{19}$$

$$\frac{d}{dZ}(\rho_L (1-\alpha) u_L^2) + F_{WL} - F_I + (1-\alpha)\frac{dP_L}{dZ} = 0. \tag{20}$$

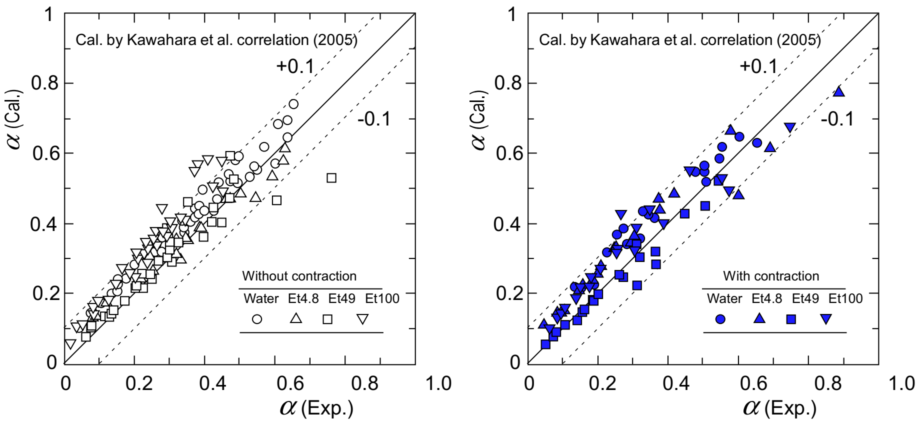

(a) Without the contraction (b) With the contraction

Fig. 15. Comparison of void fraction between experiment and calculation by Kawahara et al. correlation (2005b).

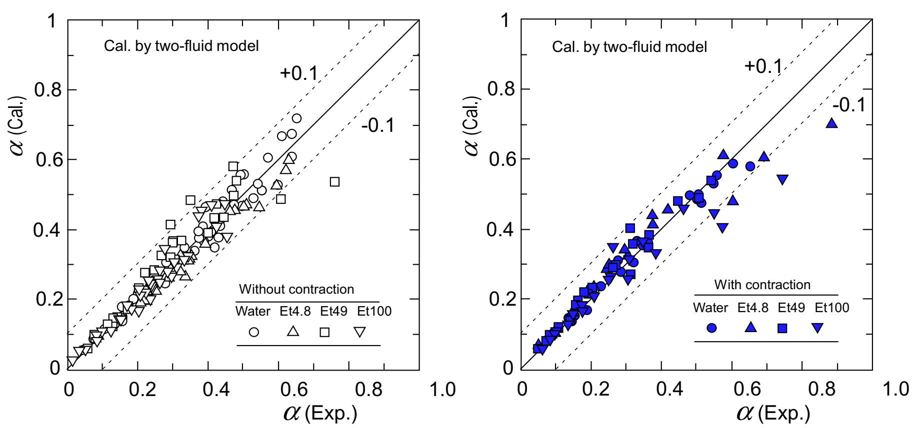

(a) Without contraction (b) With contraction

Fig. 16. Comparison of void fraction between experiment and calculation by the two-fluid model.

Table 7
Mean and RMS errors of two-fluid model for predicting void fraction.

	Distilled water		Ethanol 4.8 wt%		Ethanol 49 wt%		Ethanol 100 wt%	
	E_m	E_{rms}	E_m	E_{rms}	E_m	E_{rms}	E_m	E_{rms}
Without contraction	−0.001	0.030	−0.026	0.037	0.020	0.068	0.001	0.029
With contraction	−0.008	0.028	0.004	0.065	0.016	0.032	−0.028	0.074

Here, u_k is the mean velocity of k-phase ($k = G$ for gas, $k = L$ for liquid), F_{Wk} and F_I the wall friction force of k-phase and the gas–liquid interfacial friction force per unit volume. In the present calculation, the wall friction force for the gas phase, F_{WG}, was taken to be zero by considering the present experimental range. Thus, correlations of F_I and F_{WL}, being the same as two-phase frictional pressure drop, were required as the constitutive equations.

In our previous study on the prediction of F_I in a triangle tight lattice subchannel, having about 3 mm in hydraulic diameter (Kawahara et al., 2008), the following Tomiyama et al.'s correlation (1993) showed the best results.

$$F_I = \frac{1}{8} a_{INT} C_D \rho_L (u_G - u_L)|u_G - u_L|, \tag{21}$$

$$a_{INT} C_D = \frac{8\{\alpha(1-\alpha)(\rho_L - \rho_G)g - (1-\alpha)F_{WG} + \alpha F_{WL}\}}{\rho_L u_R |u_R|}, \tag{22}$$

$$u_R = \frac{V_{Gj} + (C_0 - 1)u_L}{1 - C_0 \alpha}, \tag{23}$$

So, Tomiyama et al.'s F_I correlation was used in this study. For C_0, we used Eq. (7) developed in this study. For F_{WL}, on the other side, we used the L–M model with the developed C correlation, Eq. (14), being the best in Section 4.1.

Fig. 16 shows a comparison of void fraction between experiment and calculation by the above two-fluid model. In the calculation of F_I by Eqs. (21)–(23), V_{Gj} and F_{WG} are taken as zero. Table 7 shows the mean and the RMS errors of the two-fluid model calculation. The calculation could predict the data within RMS error of 0.08 for both flows without and with the contraction, irrespective of working liquids.

5. Conclusions

The characteristics of adiabatic two-phase flows in a horizontal circular microchannel have been investigated experimentally and analytically. In the experiments, in order to determine the effects of fluid properties on the flow characteristics, distilled water and aqueous solutions of ethanol having three different mass concentrations were used as the working liquids. One of the four liquids and nitrogen gas were injected through a T-junction type mixer to the test microchannel made of fused silica. To know the effects of flow contraction at the channel inlet, two mixers of different inner diameters of $D_M = 250$ μm and 500 μm were used at a fixed microchannel diameter of $D = 250$ μm. In the analysis, the two-phase frictional pressure drop and the void fraction correlations from literatures were tested against the present data. Furthermore, on the void fraction, an analytical code based on a steady state, adiabatic one-dimensional two-fluid model was also tested. The main findings are as follows.

(1) The bubble velocity, u_G, depends on both the liquid properties and the flow contraction, i.e., the distribution parameter, C_0, in the drift flux model increased with increasing of the liquid viscosity and/or decreasing of surface tension, and were higher for the flows with the contraction. The C_0 data were correlated well with three dimensionless numbers, i.e., Bond number, Bo, liquid Reynolds number, Re_L, and gas Weber number, We_G.
(2) For the flows with the contraction, bubbles were elongated and flowed faster, thus the void fraction became lower.
(3) The void fraction decreased with increasing of the liquid viscosity and/or decreasing of the surface tension because the bubbles flowed faster with increasing of the liquid viscosity and/or decreasing of the surface tension.
(4) Two-phase friction multiplier in Lockhart and Martinelli (L–M) method (1949) was lower for the flows with the contraction than that without the contraction.
(5) L–M method with a newly developed C correlation accounting liquid properties and Qu and Mudawar's one (2003) gave the best prediction for the present data for both flows without and with the flow contraction, irrespective of working liquids.
(6) Armand type correlation (Armand, 1946; Chisholm, 1973; Spedding and Chen, 1986) and Kawahara et al.'s correlation (2005b) could predict well the present void fraction data.
(7) On the void fraction, two-fluid model code also could predict well the data when Tomiyama et al.'s F_I correlation (1993) with the newly developed correlations of C_0 and F_W were incorporated.

Acknowledgement

The present study was supported by KAKENHI (19560177).

References

Agostini, B., Revellin, R., Thome, J.R., 2008. Elongated bubbles in microchannels. Part I: Experimental study and modeling of elongated bubble velocity. International Journal of Multiphase Flow 34, 590–601.
Ali, M.I., Sadatomi, M., Kawaji, M., 1993. Two-phase flow in narrow channels between flat plates. Canadian Journal of Chemical Engineering 71, 657–666.
Armand, A.A., 1946. The resistance during the movement of a two-phase system in horizontal pipes. Izv. Vses. Teplotekh. Inst. 1, (AERE-Lib/Trans 828), pp. 16–23.
Beattie, D.R.H., Whalley, P.B., 1982. A simple two-phase flow frictional pressure drop calculation method. International Journal of Multiphase Flow 8, 83–87.
Butterworth, D., 1975. A comparison of some void-fraction relationships for co-current gas–liquid flow. International Journal of Multiphase Flow 1, 845–850.
Chisholm, D., 1973. Void fraction during two-phase flow. Journal of Mechanical Engineering Science 15, 235–236.
Chisholm, D., Laird, A.D.K., 1958. Two-phase flow in rough tubes. Transactions of ASME 80 (2), 276–286.
Chung, P.M.-Y., Kawaji, M., Kawahara, A., Shibata, Y., 2004. Two-phase flow through square and circular microchannels – effects of channel geometry. Transactions of ASME, Journal of Fluids Engineering 126, 546–552.
Chung, P.M.-Y., Kawaji, M., 2004. The effect of channel diameter on adiabatic two-phase flow characteristics in microchannels. International Journal of Multiphase Flow 30, 735–761.
Cicchitti, A., Lombardi, C., Silvestri, M., Solddaini, G., Zavalluilli, R., 1960. Two-phase cooling experiments – pressure drop, heat transfer and burnout measurement. Energia Nuclear 7 (6), 407–425.
Dukler, A.E., Wicks III, Moye, Cleveland, R.G., 1964. Pressure drop and hold-up in two-phase flow. AIChE J. 10 (1), 38–51.
Ishii, M., 1975. Themo-Fluid Dynamics Theory of Two-Phase Flow. Eyrolles, Paris.
Ishii, M., Mishima, K., 1984. Two-fluid model and hydrodynamic constitutive relations. Nuclear Engineering and Design 82, 107–126.
Jähnisch, K., Baerns, M., Hessel, V., Ehrfeld, W., Haverkamp, V., Löwe, H., Wille, Ch., Guber, A., 2000. Direct fluorination of toluene using elemental fluorine in gas/liquid microreactors. Journal of Fluorine Chemistry 105, 117–128.
Kawahara, A., Chung, P.M.-Y., Kawaji, M., 2002. Investigation of two-phase flow pattern, void fraction and pressure drop in a microchannel. International Journal of Multiphase Flow 28, 1411–1435.
Kawahara, A., Sadatomi, M., Okayama, K., Kawaji, M., 2003. Effects of liquid properties on pressure drop of gas–liquid flows through a microchannel. Thermal Science and Engineering 11, 25–33.
Kawahara, A., Sadatomi, M., Okayama, K., Kano, K., 2004. Pressure drop for gas–liquid two-phase flow in microchannels – effects of channel size and liquid properties. In: Proceedings of the Third International Symposium on Two-Phase Flow Modelling and Experimentation, 8 Pages in CD-ROM.
Kawahara, A., Sadatomi, M., Okayama, K., Kawaji, M., Chung, P.M.-Y., 2005a. Effects of channel diameter and liquid properties on void fraction in adiabatic two-phase flow through microchannels. Heat Transfer Engineering 26, 13–19.
Kawahara, A., Sadatomi, M., Okayama, K., Kawaji, M., 2005b. Assessment of void fraction correlations for adiabatic two-phase flows in microchannels. In: Proceedings of the Third International Conference on Microchannels and Minichannels, 8 Pages in CD-ROM.
Kawahara, A., Sadatomi, M., Kumagae, K., 2006. Effects of gas–liquid inlet/mixing conditions on two-phase flow in microchannels. Progress in Multiphase Flow Research 1, 197–203.
Kawahara, A., Sadatomi, M., Shirai, H., 2008. Two-phase wall and interfacial friction forces in triangle tight lattice rod bundle subchannel. Journal of Power and Energy Systems 2, 283–294.
Kawaji, M., Kawahara, A., Mori, K., Sadatomi M., Kumagae, K., 2006. Gas–liquid two-phase flow in microchannels: the effects of gas–liquid injection methods. In: Proceedings of the 18th National and Seventh ISHMT–ASME Heat Transfer Conference, pp. 80–89.
Lee, H.J., Lee, S.Y., 2001. Pressure drop correlations for two-phase flow within horizontal rectangular channels with small height. International Journal of Multiphase Flow 27, 783–796.
Lin, S., Kwork, C.C.K., Li, R.Y., Chen, Z.H., Chen, Z.Y., 1991. Local frictional pressure drop during vaporization for r-12 through capillary tubes. International Journal of Multiphase Flow 17, 95–102.
Lockhart, R.W., Martinelli, R.C., 1949. Proposed correlation of data for isothermal two-phase two-component flow in pipes. Chemical and Engineering Progress 45, 39–48.
McAdams, W.H., 1954. Heat Transmission, third ed. McGraw-Hill, New York.
Mishima, K., Hibiki, T., 1996. Some characteristics of air–water two-phase flow in small diameter vertical tubes. International Journal of Multiphase Flow 22, 703–712.
Owens, W.L., 1961. Two-phase pressure gradient. In: International Developments in Heat Transfer, ASME Paper No. 41, Part II, pp. 363–368.
Qu, W., Mudawar, I., 2003. Flow boiling heat transfer in two-phase microchannel heat sinks – II. Annular two-phase flow model. International Journal of Heat and Mass Transfer 46, 2773–2784.
Serizawa, A., Feng, Z., Kawara, Z., 2002. Two-phase flow in microchannels. Experimental Thermal and Fluid Science 26, 703–714.
Spedding, P.L., Chen, J.J.J., 1986. Hold-up in multiphase flow. Encyclopedia of Fluid Mechanics 3, 492–531.
Tomiyama, A., Furutani, N., Sakaguchi, T., 1993. Numerical stability of the one-pressure steady two-fluid model. Transactions of JSME (Part B) 59, 1071–1078.
Yen, T.J., Fang, N., Zhang, X., Lu, G.Q., Wang, C.Y., 2003. A micro methanol fuel cell operating at near room temperature. Applied Physics Letters 83, 4056–4058.
Zuber, N., Findlay, J.A., 1968. Average volumetric concentration in two-phase flow system. Transactions of ASME, Journal of Heat Transfer 87, 453–468.